Development of a Concrete Floating and Delamination Detection System Using Infrared Thermography

Pang-jo Chun and Shogo Hayashi

***Abstract*—Spalling of concrete fragments due to the deterioration of concrete structures can cause property damage or serious and even fatal accidents; thus, there is a need to detect such deterioration. Generally, the hammering test is employed as the main inspection method to prevent such concrete spalling; however, it requires close contact with the structure being tested. Getting close to the structure for inspection is expensive and time consuming, and if the structure is high up, there is a risk of falling. Therefore, in this study, we developed a system for inspecting concrete structures without approaching them, using infrared thermography. In order to detect floating and delamination using infrared thermography, it is necessary to find temperature irregularities caused by such damage from an infrared image, but such an inspection method has not been realized so far. There are two main reasons for this. First, it is difficult to evaluate whether the concrete structure is in an appropriate temperature condition suitable for detecting the floating and delamination. Second, it is difficult to detect temperature irregularities caused by floating and delamination among the various causes of temperature irregularities. In this study, we resolved these issues by developing equipment to investigate whether the object is in an appropriate temperature condition for proper photography and by developing a machine learning-based method to automatically detect only the temperature irregularities caused by floating and delamination. By resolving these issues, we have developed a promising novel inspection method for the prevention of concrete spalling, which is reported in this article.**

***Index Terms*—Boosting, civil engineering, concrete, infrared surveillance, inspection, machine learning.**

I. Introduction

DETERIORATION of concrete structures, including bridges, is a problem in many countries around the world. In Japan, for example, most structures built during the high economic growth period (1960–1970s) are already aging. According to the Ministry of Land, Infrastructure, Transport, and Tourism in Japan, by 2028, half of the bridges will be more than 50 years old and will start deteriorating; by 2033, two-thirds of all bridges will have been affected [1]. Additionally, according to the ASCE (American Society of Civil Engineers) infrastructure report card published in 2017, approximately 40% of the 614387 bridges in America are more than 50 years old [2]. Concrete is a brittle material consisting of water, cement, and aggregates such as crushed stone or sand. It is resistant to compression but weak in tension. The cement gradually reacts with the water and connects the aggregates, reaching its optimal design strength in about a month. There are many problems caused by the deterioration of concrete structures. In this study, we developed an inspection method to prevent concrete spalling, which is one of the most serious problems.

Spalling of concrete fragments occurs frequently. For example, on August 24, 2019, 1.3 tons of concrete fragments peeled off a bridge managed by the West Japan Railway Company due to steel rebar corrosion and fell onto a passenger vehicle passing directly below it. If concrete fragments fall and land on pedestrians and vehicles passing underneath, large-scale accidents, including fatal ones, could result. In the guidelines for regular inspections of bridges in Japan, the discovery of floating and delamination is required to prevent the occurrence of such accidents. Floating and delamination are damage in which the surface of the concrete and the interior of the concrete lose their integrity. Although the terms floating and delamination are similar, the distinction between them is that concrete fragments do not fall when subjected to a strong impact (floating) and fall (delamination).

A hammering inspection is the traditional method for detecting floating and delamination; in this method, the surface of the concrete is struck with a hammer [3]–[6]. In the test, if an abnormal noise is produced, it indicates that floating or delamination may have occurred, and the test is considered to be very reliable. However, as the hammer test can only be used to inspect the location hit by the hammer, it requires that all areas of the structure be exhaustively struck to inspect an entire bridge which entails considerable labor. Additionally, when inspecting parts of a bridge situated at high locations, it is not easy to get close to them to perform the hammering test. Methods

Manuscript received January 26, 2021; revised May 7, 2021; accepted August 18, 2021. Date of publication September 10, 2021; date of current version December 15, 2021. Recommended by Technical Editor C. C. Cheah. (*Corresponding author: Pang-jo Chun.*)

Pang-jo Chun is with the Department of Civil Engineering, The University of Tokyo, Tokyo, 113-8654, Japan (e-mail: chun@g.ecc.u-tokyo.ac.jp).

Shogo Hayashi is with the West Nippon Expressway Engineering Shikoku Company Limited, Takamatsu 760-0072, Japan (e-mail: shogo.hayashi@w-e-shikoku.co.jp).

Color versions of one or more figures in this article are available at https://doi.org/10.1109/TMECH.2021.3106867.

Digital Object Identifier 10.1109/TMECH.2021.3106867

(a) (b)

Fig. 1. Example of inspection using (a) rope access and (b) high-location work vehicle for bridge inspection.

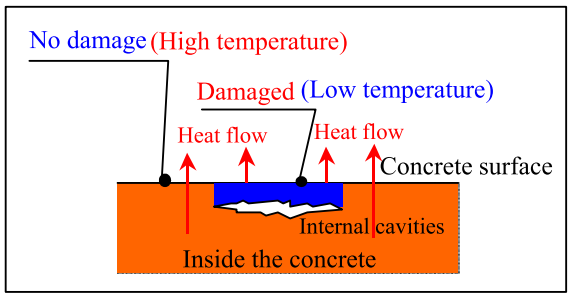

Fig. 2. Temperature unevenness when the concrete temperature is higher than the external temperature.

to approach high up include, for instance, rope access [see Fig. 1(a)] or using a high-location work vehicle [see Fig. 1(b)]; however, these methods are costly and highly dangerous. Hence, there is a need for inspection methods that can be performed remotely from the ground and with less effort, and that can be applied to the entire structure with high precision. In Japan, as a part of CIM (construction information modeling/management), the utilization of information-based techniques such as image analysis technology, artificial intelligence (AI) technology, and cloud servers has been promoted. This study aims to use this framework to make the inspection of floating and delamination more efficient.

As for the detection of concrete damage using image analysis and AI technologies, much research has been conducted on the detection of cracks in visible images [7]–[11]. However, since floating and delamination often proceed from the inside, they are undetectable from the analysis of visible images. On the other hand, considering that the temperature distribution caused by floating and delamination is different from the surrounding area due to the internal cavities as shown in Fig. 2, the use of infrared images is effective. In fact, such infrared images have been utilized for studying tile delamination and similar activities [12], [13]. In [12], mathematical investigations and experiments showed that tile delamination can be detected by an infra-red camera, and in [13], the appropriate camera performance for detecting tile delamination was investigated and then damage detection was performed in a real building. However, the temperature distribution of concrete structures targeted in this study is less clear than that of tiles, which makes detection more difficult. The authors in [14]–[16] worked on the detection of floating and delamination in concrete structures with such a complex temperature distribution. A significant study in [14] shows the effect of various delamination features on detection accuracy through precise experiments using full-scale specimens. However, the authors only mention that the automatic detection method using machine learning is promising. Ellenberg *et al.* [15] describe an inspection by UAV equipped with an infra-red camera, which is a very promising application; however, the automatic detection in this study did not use machine learning and was limited to detecting only damaged areas that could be found from simple image processing. Similarly, Sultan and Washer [16] define thresholds based on experimental situations and only uses simple image processing to determine damage. However, the actual temperature irregularities caused by floating and delamination are complex, and simple image processing such as fixing thresholds and parameters can cause errors, especially if the structure changes. In addition, since there are many factors other than floating and delamination that cause temperature irregularities, human judgment is currently required to distinguish between these factors. However, in order to improve the efficiency of inspection, automation is necessary; therefore, this research aims to realize an automated damage detection system. Such a system has not been achieved so far for two major reasons. First, it is difficult to assess whether the concrete structure is in an appropriate temperature condition for the detection of floating and delamination from an infrared image to be possible. Second, no methodology has been established for automatically selecting temperature irregularities due to floating and delamination from a large array of temperature irregularities in infrared images. The purpose of this study is to develop a method for detecting floating and delamination of concrete structures using an infrared camera by resolving the above-mentioned two issues. The former issue was resolved by developing an instrument to examine the temperature condition of concrete structures that is suitable for detecting floating and delamination, whereas the second issue was resolved by developing an automatic detection method using a LightGBM (Light Gradient Boosting Machine), a machine learning method, after constructing a cloud server system that collects and accumulates data from many operators.

With the realization and implementation of this system, it is now possible to automatically detect floating and delamination from infrared images with high accuracy, and to take efficient measures to prevent spalling. A total of more than 3 million m^2 was surveyed in Japan and the USA using this system, and the effectiveness of the system has been confirmed by practitioners. Thanks to such extensive inspection works by many inspectors, data have been accumulated, contributing to further improvements in accuracy. Details of the developed equipment and technology for detecting floating and delamination with high accuracy are presented in the subsequent sections.

II. Acquiring Infrared Images Using an Infrared Camera

A. Experiment for Selecting the Infrared Camera

In this section, we first determined the required performance of an infrared camera to acquire infrared images. These images are necessary for the detection of floating and delamination.

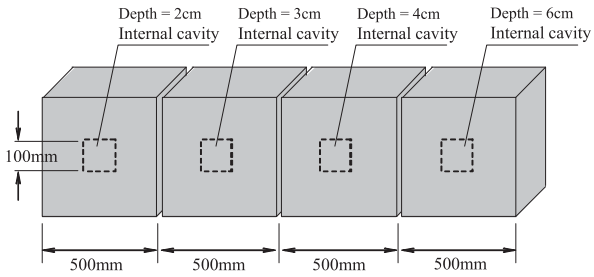

Fig. 3. Concrete specimens and the positions and depths of the cavity.

TABLE I
INFRARED CAMERAS USED IN THE COMPARISON TEST

Product name	SC6000 (FLIR)	FLIR SC660 (FLIR)
Infrared image resolution	640 × 512	640 × 480
Infrared detecting element	Indium antimonide	Microbolometer
NETD	0.02–0.03 K	0.06–0.08 K

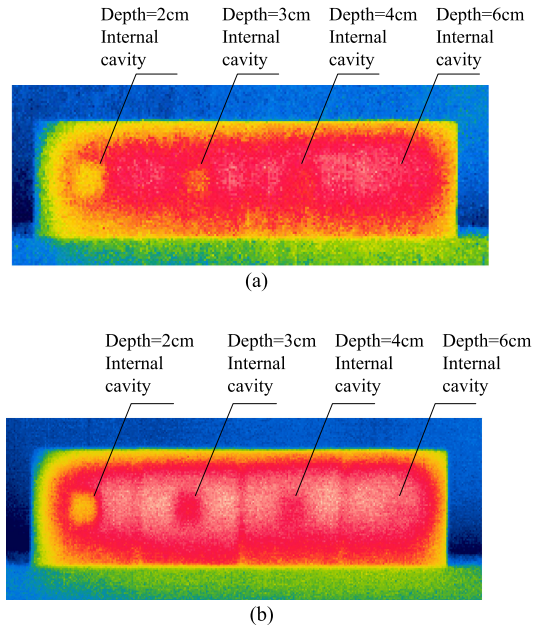

Fig. 4. Thermal images of concrete specimen with cavities. (a) Capture results using SC660. (b) Capture results using SC6000.

Although there are many performance parameters for infrared cameras, such as the number of pixels and the frame rate, the noise equivalent temperature difference (NETD) is the most important performance parameter when considering the detection of temperature irregularities caused by floating and delamination. In order to detect this damage, the temperature difference in the floating and delamination region needs to be larger than the NETD of the infrared camera. In this study, we used specimens with varying depths of cavities to compare the infrared images obtained using the infrared cameras with different NETDs and then investigated the required NETD performance based on the obtained results.

1) Creating Specimens With Cavities: The test specimens were provided with cavities of 100 mm x 100 mm ($t = 10$ mm) at depths of 20, 30, 40, and 60 mm from the surface (see Fig. 3). These depths were determined based on the general rebar cover thickness of 30–40 mm in the superstructure of concrete bridges. The specimens were installed in shaded areas below bridges and photographed at 11 PM when the diurnal temperature was $\geq$7 °C. The reason for doing the photography at night was to create temperature irregularities around the cavity, as shown in the mechanism in Fig. 2.

2) Infrared Camera Comparison: In order to investigate the effect of the difference in NETD on the detection performance, the two types of cameras shown in Table I were placed side by side and the specimens were photographed simultaneously.

The major difference between the SC6000 and the SC660 lies in the NETD. This difference is caused by the difference in the detecting element installed in the infrared camera. An infrared camera using an uncooled micro bolometer as a detector obtains a temperature distribution based on the principle of converting thermal energy into electrical resistance, but in such a case, the temperature resolution is generally in the range of 0.06 to 0.08 K. On the other hand, when indium antimonide is used as a detector, the detection sensitivity is high because it detects electrical phenomena caused by light energy, and the temperature resolution is 0.02–0.03 K. In addition, the response speed of such a system is fast.

The results are shown in Fig. 4, where the infrared image of SC6000 with the minimum detection temperature of 0.02–0.03 K can detect damage as deep as 40 mm, whereas the image of SC660 cannot detect the damage except at a depth of 20 mm. These results indicate that the variation in NETD makes a significant difference to the detection of floating and delamination. In particular, for the detection of defects 40 mm in depth required for concrete bridges, it is necessary to use an infrared camera with a cooled indium antimonide detector. On the other hand, it was found that defects at a depth of 60 mm could not be detected. However, considering that the typical rebar cover thickness of bridge superstructures is 40 mm, it can be said that this method is suitable for detecting floating and delamination in concrete structures.

B. Methods for Evaluating the Thermal Environment in Actual Structures

Although we determined the required performance of infrared cameras using the specimens in the previous section, heat flows in actual structures are complex and the environmental conditions change. Consequently, there is no guarantee that floating and delamination can be detected as expected. Therefore, we developed a concrete specimen (hereafter, "attachable specimen"), which can be directly attached to a bridge to evaluate the thermal condition and thereby confirm if the concrete structure is in the appropriate capture environment.

The attachable specimen consists of a 30 cm x 30 cm concrete plate with a thickness of t cm and a 1-mm thick thermal conductive sheet. By attaching the attachable specimen to the bridge, a simulated internal cavity of 10 cm × 10 cm in size and 1 mm in

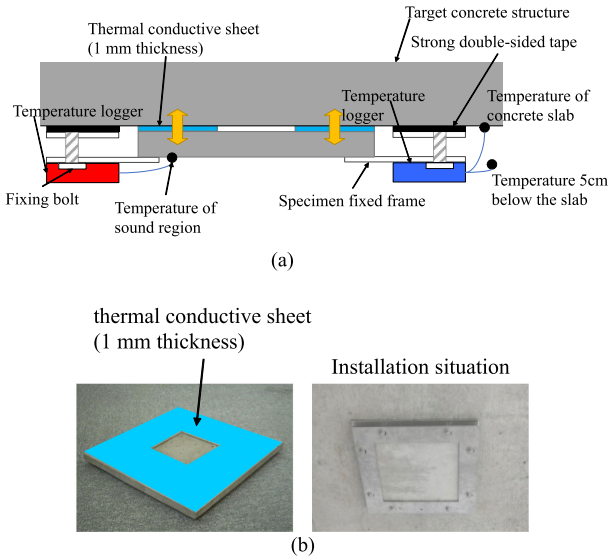

Fig. 5. Structure and installation situation of attachable specimen. (a) Structure of attachable specimen. (b) Installation situation.

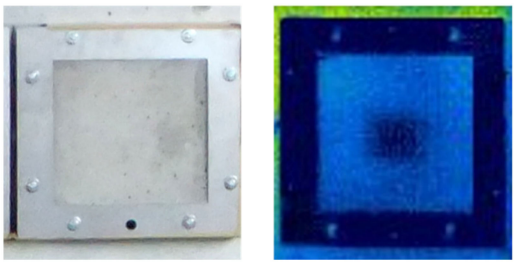

Fig. 6. Visible image and thermal image of attachable specimen ($t = 3$ cm).

thickness can be created in the investigated concrete structure at an arbitrary depth (t cm) (see Fig. 5). The heat conduction sheet between the concrete plate and the concrete structure allows the attachable specimen to be thermally integrated with the concrete structure. If this simulated damage can be detected by the infrared camera, then the temperature condition is appropriate for detecting actual damage at a similar depth. For example, to enable the detection of floating with a depth of 3 cm, t can be set as 3 cm. An example of the detection of a simulated cavity is shown in Fig. 6. The appearance of the cavity with a depth of 3 cm that cannot be determined from a visible image can be determined by the temperature difference in the central section when looking at the infrared image.

In addition, to confirm whether the thermal conductive sheets are really functioning to form a thermally integrated structure, we attached the attachable specimen to the bridge and measured the temperature. On good days, when the diurnal temperature range was $\geq$7 °C, temperature measurements were conducted every hour of the lower surface of the concrete bridge slab, areas 5-cm below the lower surface of the slab, the Stevenson screen installed around the bridge abutment, and the sound area of the attachable specimen. Fig. 5(a) shows the temperature measurement position of the attachable specimen, and Fig. 7

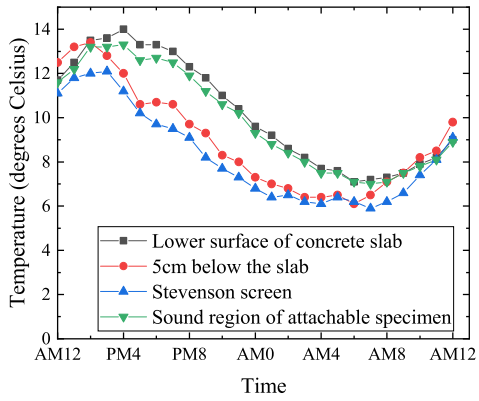

Fig. 7. Attachable specimen verification results.

shows the measurement results. The temperature of the lower surface of the concrete bridge slab and that of the sound area of the attachable specimen showed the same transition, indicating that the concrete bridge and attachable specimen were thermally integrated. After confirming that the concrete structure is in an appropriate thermal environment using the attachable specimen, internal damage can be detected from thermal images. In the next section, a method to select which of the detected temperature irregularities are due to floating or delamination by machine learning is presented.

III. Method for Detecting Damage Using Machine Learning

The infrared thermography method has the problem of missing or incorrectly detecting floating and delamination when the inspector manually evaluates these from infrared images. To resolve this issue, we constructed a system in which floating and delamination in infrared images can be automatically and accurately detected using machine learning.

A. Data Collection

In order to improve the accuracy of a classifier developed by machine learning methods, it is necessary to train it using a large amount of data obtained in various environments. However, there is a limitation to the amount of data that can be collected by our institution alone, so we have built a cloud server, as shown in Fig. 8, which is a system for collecting data from users who have performed inspections in various environments. This improves the accuracy of the system, which is of great benefit to the users. The details of the data collection procedure are as follows.

1) Upload the infrared image to the cloud server.
2) The cloud server analyzes the image and returns the results to the user.
3) Whether the answers given by the system are really correct will be revealed during detailed inspections and repairs. The results are returned to the cloud server.
4) The classifier is periodically retrained using the newly stored results in the cloud server to improve its accuracy.

This system is frequently used by the Nippon Expressway Company, which manages most of the expressways in Japan, and

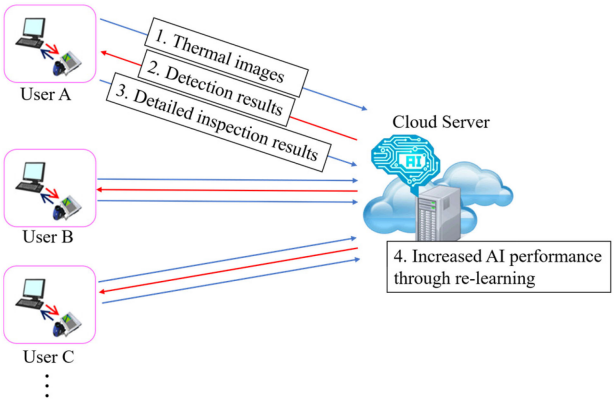

Fig. 8. Link between cloud server and user.

the Honshu–Shikoku Bridge Expressway, which manages many long-span bridges, so data are collected at various locations in various environments. Until now, a total of 4139 sets of data have been collected from reinforced concrete bridges, steel bridges, and box girder bridges.

B. Detection of Floating and Delamination Using Machine Learning

1) Overview: In this section, we describe a method for developing a classifier for detecting floating and delamination from the obtained infrared images using machine learning. Even if a thermal irregularity is discovered in the infrared image, it does not necessarily mean that the area has floating or delamination damage. For example, on the surface of concrete structures, free lime adhesion is generated by rainwater infiltration, and unevenness created during construction, which causes temperature irregularities. Therefore, machine learning is used to determine whether the cause of the temperature irregularity is floating or delamination, or something else. Table II shows the factors that cause temperature irregularities and gives a comparison between visible and infrared images in each case. The details of each factor are described in the next section.

2) Factors Causing Temperature Unevenness:

a) Floating Area: A floating area is a place where an abnormal noise can be heard when the area is struck with an inspection hammer, although no concrete fragments fall off. As shown in Table II, although these floating areas are difficult to discern from visible images, the temperature irregularities can be confirmed from infrared images.

b) Delamination Area: A delaminated area is an area where concrete fragments fall off when the location is struck with an inspection hammer. Although the appearance of the infrared image is different from that of the floating area, clear temperature irregularities can also be observed.

c) Adhered Slag: Slag adhering to formwork joints during concrete casting is 2–5-mm thick, so it can be clearly detected by infrared thermography as elongated temperature changes along the joints. The shape of the slag is clearly different from that of the floating area and the delamination area.

TABLE II
FACTORS CAUSING TEMPERATURE IRREGULARITIES

Factors	Visible images	Infrared images
Floating area		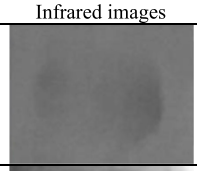
Delamination area		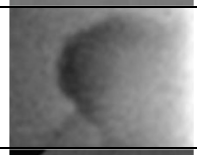
Adhered slag		
Foreign substances		
Repair marks		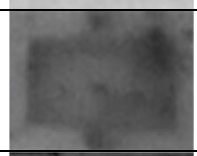
Free lime		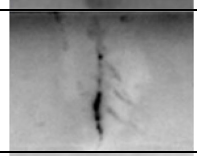
Sound area		

d) Foreign Substances: If foreign substances such as wood fragments, and other, enter the cover concrete, they can be detected as temperature irregularities from infrared images. The image in Table II shows an area in which wooden fragments have infiltrated. As with the adhered slag, the shape of foreign substances differs from the floating area and the delamination area.

e) Repair Marks: When concrete is broken, it is repaired with a material such as nonshrinking mortar. Since the thermal conductivity of the repair material is generally different from that of the concrete, a temperature irregularity occurs. The figure in Table II shows an example of temperature irregularities at the site of a cross-sectional repair. In this case, a rectangular shape is often detected.

f) Free Lime: When free lime adheres to the concrete surface, it is detected as a peculiar temperature irregularity. This is due to the fact that the reflectance and thermal conductivity of the free lime are different from those of the sound concrete, and that there is space between the free lime and the concrete. The figure in Table II shows a case with free lime of approximately $t = 1$ mm.

g) Sound Area: This is a case in which temperature irregularities appear in a sound section. This may happen for example, if the concrete is wet or dirty, which changes the solar energy absorption rate. Table II shows some examples of this.

C. Classification Based on Machine Learning

Here, cases (1)–(7) are classified using a machine learning technique. As a result of trying various methods by trial and error, we found that the most accurate method was a rather classical one, which is to quadratize the infrared image and then classify it by LightGBM [17] using shape features. Note that the authors have been actively conducting research on damage detection and evaluation using deep learning [18], [19], and also tried to use methods such as YOLOv5 in this study, but were unable to obtain sufficient accuracy. This may be due to the fact that the amount of infrared image data was still not sufficient for YOLOv5 and other deep learning methods to find features by themselves. Although this may be resolvable by accumulating data in future, we will not use it in this article. On the other hand, the method proposed in this study is considered to be sufficiently accurate even with the amount of data prepared in this study by setting the shape features to be focused on.

First, we perform quadration. As a preprocessing step, we first calculate the difference from the average value of the surrounding images using the following formula:

$$I_a(p,q) = I_b(p,q) - \frac{1}{2(n+1)^2}\sum_{l=-n}^{n}\sum_{k=-n}^{n} I_b(p+k, q+l) \tag{1}$$

where p and q denote the position of the target pixel, I_a denotes the image after correction, and I_b denotes the image before the correction. We set this I_a threshold value to 0.12 °C, 0.08 °C, and 0.04 °C, respectively, and perform quadration. In the following figures, the area above 0.12 °C is red, the area between 0.08 °C and 0.12 °C is yellow, the area between 0.04 °C and 0.08 °C is blue, and the area below 0.04 °C is colorless. Examples of quadratized infrared images for each of the damage types shown in Tables II and III. The figures in Table III, which show different aspects of each damage type, suggest that the shape and location of these red, yellow, and blue regions are important for damage classification. For example, if the red region is far from the center of the entire region, the possibility of delamination increases. Given this, it is expected that the distance between the centers of gravity of the red, yellow, and blue areas may function as effective feature values for classification. As shown in the schematic diagram in Fig. 9, there are three distances between the centers of gravity, namely between the red and yellow areas (d_{RY}), between the red and blue areas (d_{RB}), and between the yellow and blue areas (d_{YB}).

In addition, the shapes of the red, yellow, and blue areas are also important. In particular, the occupancy rate, complexity, and circularity promise to function as means of judging the infiltration of foreign substances and repair marks; therefore, they have been included as feature values in this study.

$$\text{occupancy rate}_\text{i} = \frac{S_i}{h_i \times w_i}(i = R, R+Y, R+Y+B)$$

TABLE III
TREND OF QUADRATIZED INFRARED IMAGES FOR EACH DAMAGE

Each damage type	Infrared image after quadrature	General trend of shapes
Floating area	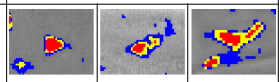	The shape of the periphery is smooth, and the center of gravity of the red area is near the center.
Delamination area	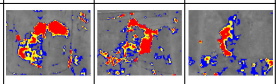	The shape of the periphery is complex, and the center of gravity of the red area deviates from the center.
Adhered slag	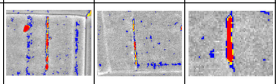	The shape of the periphery is complex, and the entire area is long and narrow.
Foreign substances	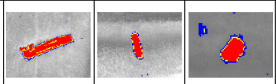	The shape is square, and the red colored area occupies a large proportion of entire shape.
Repair marks	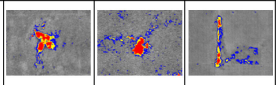	The shape varies depending on the repair area. The proportion of red and yellow area are large.
Free lime	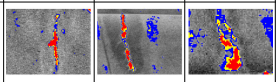	The shape of the periphery is complex, and the proportion of red area is large.
Sound area	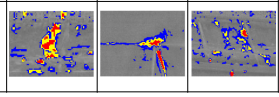	The shape varies, and the yellow and blue area occupy a large proportion.

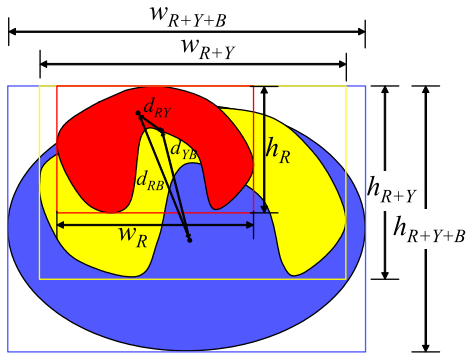

Fig. 9. Schematic showing calculation of shape feature values for a quadrated image.

$$\text{complexity}_\text{i} = \frac{L_i}{S_i}(i = R, R+Y, R+Y+B)$$
$$\text{circularity}_\text{i} = \frac{4\pi S_i}{{L_i}^2}(i = R, R+Y, R+Y+B). \tag{2}$$

In (2), L is the perimeter length, S is the area, h is the height, and w is the width. In addition, the subscripts R, $R+Y$, and $R+Y+B$ indicate the red area, the combined red and yellow areas, and the combined red, yellow, and blue areas, respectively. In other words, we can acquire a total of $3 \times 3 = 9$ feature values from (2).

In addition, the co-occurrence matrix [20], which is another texture analysis method that can quantify the light and shade changes in an image was used. As shown in Fig. 10, the method calculates a probability matrix whose elements are the probabilities $P_\delta = (c_i, c_j)$ that the pixel value of a point at a distance of a certain displacement $\delta = (r, \theta)$ from a point with pixel value

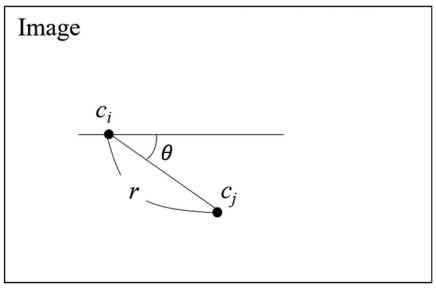

Fig. 10. Relationship between two points on the co-occurrence matrix.

c_i is c_j. From this matrix, it is known that several features can be calculated.

Here, in particular, we will calculate a total of four feature values, namely variance, sum average, sum variance, and contrast, as defined in (3). Variance represents the size of the distribution of the image as a whole, so it can be used to evaluate the disparity between light and darkness. Because the sum average is the sum of the pixel value changes of the two points, k, multiplied by the probability of the case, the value of sum average is larger for images with large pixel value changes. Sum variance is the square of the difference between k and the sum average, so this value will be small in a uniform image. Additionally, contrast evaluates the local variance in light and darkness in the image. Here, as for the damage classification, change and disparity in the light and darkness are considered to be important variables; thus, it is reasonable that these should be used as feature values.

$$\begin{aligned}
\text{Variance} &= \sum_{i=0}^{n-1}\sum_{j=0}^{n-1}(1-\mu_x)^2 P_\delta(i,j) \\
\text{Sum average} &= \sum_{k=0}^{2n-2} k P_{x+y}(k) \\
\text{Sum Variance} &= (k-\text{Sum average})^2 P_{x+y}(k) \\
\text{Contrast} &= \sum_{k=0}^{n-1} k^2 P_{x-y}(k). \qquad (3)
\end{aligned}$$

Here,

$$\begin{aligned}
\mu_x &= \sum_{i=0}^{n-1}(iP_\delta(i,j)) \\
P_{x+y}(k) &= \sum_{i=0}^{n-1}\sum_{j=0}^{n-1} P_\delta(i,j) \quad \text{where } i+j=k \\
P_{x-y}(k) &= \sum_{i=0}^{n-1}\sum_{j=0}^{n-1} P_\delta(i,j) \quad \text{where } |i-j|=k.
\end{aligned}$$

In this study, r in $\delta = (r, \theta)$ was set to two patterns 1 or 2, and θ was set to eight patterns 0°, 45°, 90°, 135°, 180°, 225°, 270°, and 315°, then the mean value using (3) for each of the values of r and θ was set as the feature value. In other words, there are four feature values (variance, sum average, sum variance, and contrast) obtained from the co-occurrence matrix in (3).

TABLE IV
PARAMETERS USED IN LIGHTGBM

Number of iterations	1,000
Early stopping	10
Number of leaves	200
Learning rate	0.02
Maximum number of bins	100
Minimum number of data entries in a leaf	10
Maximum depth	Unlimited
Loss function	Multiclass logarithmic loss

TABLE V
ANALYSIS RESULTS (7 CLASSES)

Analysis result \ Hammering test	(1)	(2)	(3)	(4)	(5)	(6)	(7)	Total
(1) Floating	171	16	0	8	21	10	27	253
(2) Delamination	2	184	4	2	44	21	37	294
(3) Adhered slag	4	0	138	14	21	39	10	226
(4) Foreign substances	5	3	16	102	6	38	16	186
(5) Repair marks	16	31	18	2	130	67	78	342
(6) Free lime	8	13	28	19	46	319	148	581
(7) Sound area	9	12	0	12	62	307	1855	2257
Total	215	259	204	159	330	801	2171	4139

There are other known features of the co-occurrence matrix, such as angular second moment, correlation, and difference entropy. However, as a result of exhaustive multiple comparisons using the Tukey–Kramer method, we decided not to use any of these other features, as they did not have a significant impact on improving accuracy.

From these obtained 16 features, classification was performed by the classifier trained using the supervised machine learning method. In this study, we used LightGBM, which is a gradient-boosting framework that uses tree-based learning algorithms [17]. LightGBM is also known to have the following merits: fast training speed, high efficiency, low memory usage, high accuracy, and the ability to handle large-scale data. Table IV shows the list of LightGBM parameters that were used in this study. Their details are described in [21]. However, although we examined the effect of these parameters on the accuracy, we found that doubling or halving the values did not significantly affect the results.

D. Analysis Results and Implementation

The analysis results using this method are shown in Table V. Here, the analysis performs leave-one-out cross validation. This is a validation method that trains all but one datum, and the prediction is made for that one datum. The process was repeated until the rest of the overall dataset was trained.

As can be seen from Table V, the accuracy of 70.0% (2899/4139) was obtained. It may appear that the accuracy is not very high. However, if we look at Table V, there are many mistakes that are not particularly serious. For example, there are many cases in which (6) free lime and (7) sound areas are mistaken but if the objective is to detect floating and delamination from infrared images, these mistakes do not represent a major problem. Therefore, Table VI shows the confusion matrix of a

TABLE VI
ANALYSIS RESULTS (2 CLASSES)

Hammering test / Analysis result	(1)+(2)	(3)~(7)	Total
(1)+(2)	373	174	547
(3)~(7)	101	3491	3592
Total	474	3665	4139

TABLE VII
FLOATING AND DELAMINATION DETECTION ORDER

	1st candidate	2nd candidate	3rd candidate	4th or below	Total
(1) Floating	171	44	0	0	215
(2)Delamination	184	70	5	0	259
Total	355	114	5	0	474

TABLE VIII
NUMBER OF MISJUDGMENTS AS FLOATING OR DELAMINATION

	1st candidate	2nd candidate	3rd candidate	4th or below	Total
Misjudged as floating	66	311	449	2839	3665
Misjudged as delamination	108	427	760	2370	3665

summary of (1) and (2), which we wish to detect, and the others, i.e., (3)–(7). By doing this, we can see that the high accuracy of 93.4% (3864/4139) was achieved.

However, on the other hand, there are a certain number of cases that are judged to be sound despite the fact that there is actually floating or delamination (101/474). When considering the goal of preventing concrete fragments from falling, it is necessary to keep to a minimum the cases in which actual damage is overlooked. On the other hand, judging damage to have occurred even though it has not is not a major problem compared to oversight. Therefore, after finding the top three cases, we found the probability of these occurring and presented them to the user. By doing this, it was possible to alert the inspectors to damage that was occurring, based on the situation.

In case there is actual floating and delamination, the probability of the first candidate being output by LightGBM is 78.7% (373/474). However, when we examined the results thoroughly, we found that floating and delamination were evaluated as the second candidate in many cases. Table VII shows the number of candidates for which floating and delamination are evaluated. As shown in the table, 98.9% (469/474) of the samples are included in the top two and 100% in the top three, indicating that the method demonstrates sufficient performance as a floating and delamination detection system to prevent floating and delamination from being overlooked. Table VIII shows the results of misjudgments such as floating and delamination, even though the correct answers are (3)–(7). Although there are few results that are incorrectly identified as the first candidate (66/3665 = 1.8% for floating, 108/3665 = 2.9% for delamination), there are many misjudgments when considering the first through third candidates together (826/3665 = 22.5% for floating and 1295/3665 = 35.3% for delamination), and there is still room for improvement. However, from the viewpoint of preventing serious accidents, if the number of overlooking is small, as shown in Table VII, the method is worthwhile even if there are a certain number of over detections, as shown in Table VIII.

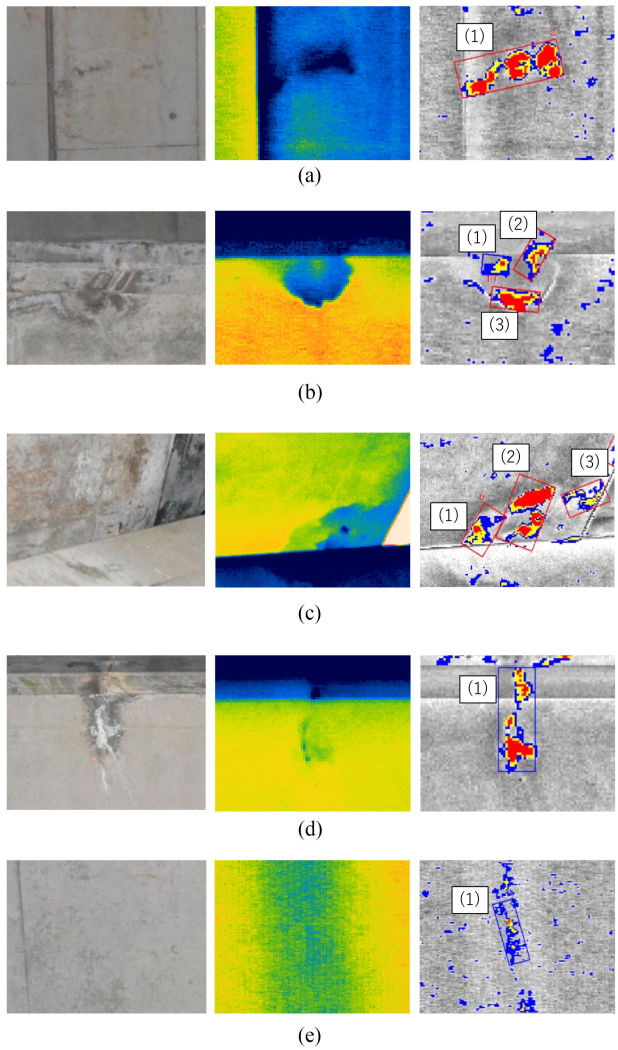

Fig. 11. Example of automatic detection results. From the left side, respectively, these are visual images, infrared images, and quadratized infrared images. The top three classification results are listed below each image. (a) Detection (1): Floating: 97.8%, Delamination: 1.2%, Free lime: 0.8%. (b) Detection (1): Free lime: 72.3%, Repair marks: 21.4%, Sound area: 6.3% Detection (2): Delamination: 82.1%, Free lime: 11.3%, Sound area: 6.1% Detection (3): Delamination: 91.3%, Free lime: 7.9%, Floating: 0.5%. (c) Detection (1): Repair marks: 41.2%, Delamination: 37.9%, Sound area: 21.0% Detection (2): Delamination: 88.0%, Free lime: 7.1%, Repair marks: 4.0% Detection (3): Delamination: 42.9%, Sound area: 39.4%, Repair marks: 17.9%. (d) Detection (1): Free lime: 72.4%, Delamination: 20.1%, Floating: 4.3%. (e) Detection (1): Sound area: 98.1%, Adhered slag: 1.1%, Repair marks: 0.8%.

Fig. 11 shows an example of the analysis results. From the left side, respectively, these are visual images, infrared images, and quadratized infrared images. Fig. 11(a) shows the result of detecting floating as the first rank. The infrared image clearly shows the existence of floating, and the detailed investigation showed that it existed. Fig. 11(b) shows a case where there

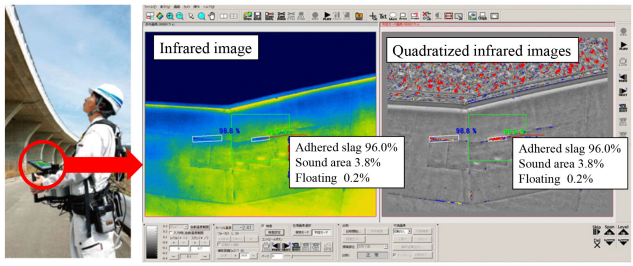

Fig. 12. Photographs taken during a bridge inspection using the developed system and the monitor displayed on the tablet. Note that the evaluation results were originally displayed in Japanese, but for this figure, they will be translated to English.

are three temperature irregularities represented by (1)–(3) in the image, where (1) was classified as free lime, and (2) and (3) as delamination. The results of the detailed investigation showed that all of these were correct. Fig. 11(c) also shows three temperature irregularities indicated as (1)–(3) in the image, and the delamination is classified as second, first, and first, respectively. According to the detailed investigation, delamination existed in all positions (1)–(3). In (1), the delamination was classified as second place, but the inspector was able to take appropriate action because it was clear from the visible image that the repair marks classified as the first place did not exist. Fig. 11(d) shows a case in which free lime is in first place, whereas Fig. 11(e) shows an example in which sound areas are in first place. Detailed investigations later proved that both results were correct. It is difficult for humans to classify these damage types from infrared images, indicating that the automatic detection method employing machine learning developed in this study works appropriately.

In addition, we implemented a system for site inspections by combining a tablet that included this analysis program with an infrared camera. Fig. 12 shows an image of an inspection that used this system and an example of the infrared image and analysis results displayed on the monitor. As shown in the figure, the system displayed the damage in a very easy-to-understand manner, and as a result of taking countermeasures based on the results, we have been able to prevent accidents involving the spalling of concrete fragments.

IV. Conclusion

In this article, we established a method for automatically detecting floating and delamination of concrete structures using infrared thermography. We accomplished this through an investigation of the required performance of an infrared camera, development of an attachable specimen to understand the thermal condition, and the development of a method for detecting damage automatically and accurately using LightGBM. This novel method has great significance even from a practical point of view; it will fundamentally change the inspection work itself and will contribute greatly to ensuring the safety of concrete structures. In order to collect a large amount of data, the system was configured to use a cloud server, which also contributed to improving the detection accuracy. This system has been used in Japan and the USA, but no case of overlooked damage has been reported so far, and this is supporting evidence of its high accuracy.

Future tasks are described as follows. This study dealt with floating and delamination of concrete, however, since civil engineering structures frequently use not only concrete but also steel members, we would like to link the developed method in this study to the detection of damage in steel members. For example, the authors have shown in [22]–[25] that corrosion and fatigue of steel members have a significant effect on the safety of structures, but an effective method to evaluate them from a distance has not been established, which is a topic that needs to be solved. Since corrosion and fatigue may affect the temperature distribution, our method using infrared images may be useful to detect them. In addition, currently, we are able to detect floating and delamination with 98.9% accuracy by including the second candidate, and 100% accuracy by including the third candidate; however, we would really like to detect them with high accuracy as the first candidate. For this purpose, it is still necessary to use the framework of deep learning, which automatically generates a large number of features, instead of manually determining the features as in this study. For this reason, we are currently collecting bridge inspection data in a wide variety of environments. In addition to this, we are also considering including visible images in the analysis. Considering that visible images also contain various types of information, we expect that simultaneous analysis of infrared and visible images will improve the accuracy and prevent errors such as (1) in Fig. 11(c).

References

[1] P. J. Chun *et al.*, "Utilization of unmanned aerial vehicle, artificial intelligence, and remote measurement technology for bridge inspections," *J. Robot. Mechatronics*, vol. 32, no. 6, pp. 1244–1258, 2020.
[2] American Society of Civil Engineers, "2017 report card for America's infrastructure," American Society of Civil Engineers (ASCE), Reston, VA, USA, 2017.
[3] N. Delatte *et al.*, "Application of nondestructive evaluation to subway tunnel systems," *Transp. Res. Rec.*, vol. 1845, no. 1, pp. 127–135, 2003.
[4] P. J. Chun *et al.*, "Random forest-based evaluation technique for internal damage in reinforced concrete featuring multiple nondestructive testing results," *Construction Building Mater.*, vol. 253, 2020, Art. no. 119238.
[5] H. Fujii, A. Yamashita, and H. Asama, "Defect detection with estimation of material condition using ensemble learning for hammering test," in *Proc. IEEE Int. Conf. Robot. Automat.*, 2016. pp. 3847–3854.
[6] V. M. Malhotra and N. J. Carino, *Handbook On Nondestructive Testing of Concrete.* Boca Raton, FL, USA: CRC Press, 2003.
[7] P. J. Chun, S. Izumi, and T. Yamane, "Automatic detection method of cracks from concrete surface imagery using two-step light gradient boosting machine," *Comput.-Aided Civil Infrastructure Eng.*, vol. 36, no. 1, pp. 61–72, 2021.
[8] T. Yamane and P. J. Chun, "Crack detection from a concrete surface image based on semantic segmentation using deep learning," *J. Adv. Concrete Technol.*, vol. 18, no. 9, pp. 493–504, 2020.
[9] A. Zhang *et al.*, "Automated pixel-level pavement crack detection on 3D asphalt surfaces using a deep-learning network," *Comput.-Aided Civil Infrastructure Eng.*, vol. 32, no. 10, pp. 805–819, 2017.
[10] Q. Zou, Z. Zhang, Q. Li, X. Qi, Q. Wang, and S. Wang, "Deepcrack: Learning hierarchical convolutional features for crack detection," *IEEE Trans. Image Process.*, vol. 28, no. 3, pp. 1498–1512, Mar. 2018.

[11] S. Bang, S. Park, H. Kim, and H. Kim, "Encoder–decoder network for pixel-level road crack detection in black-box images," *Comput.-Aided Civil Infrastructure Eng.*, vol. 34, no. 8, pp. 713–727, 2019.
[12] R. M. D. Andrade and A. C. Eduardo, "Methodology for automatic process of the fired ceramic tile's internal defect using IR images and artificial neural network," *J. Braz. Soc. Mech. Sci. Eng.*, vol. 33, no. 1, pp. 67–73, 2011.
[13] E. Bauer *et al.*, "Infrared thermography–evaluation of the results reproducibility," *Struct. Surv.*, vol. 33, no. 1, pp. 20–35, 2015.
[14] J. C. Gu, S. Unjoh, and H. Naito, "Detectability of delamination regions using infrared thermography in concrete members strengthened by CFRP jacketing," *Composite Struct.*, vol. 245, 2020, Art. no. 112328.
[15] A. Ellenberg, A. Kontsos, F. Moon, and I. Bartoli, "Bridge deck delamination identification from unmanned aerial vehicle infrared imagery," *Automat. Construction*, vol. 72, pp. 155–165, 2016.
[16] A. A. Sultan and G. Washer, "A pixel-by-pixel reliability analysis of infrared thermography (IRT) for the detection of subsurface delamination," *NDT E Int.*, vol. 92, pp. 177–186, 2017.
[17] G. Ke *et al.*, "LightGBM: A highly efficient gradient boosting decision tree," in *Proc. Adv. Neural Inf. Process. Syst.*, 2017, pp. 3146–3154.
[18] P. J. Chun, T. Yamane, S. Izumi, and T. Kameda, "Evaluation of tensile performance of steel members by analysis of corroded steel surface using deep learning," *Metals*, vol. 9, no. 12, 2019, Art. no. 1259.
[19] P. J. Chun, T. Yamane, and Y. Tsuzuki, "Automatic detection of cracks in asphalt pavement using deep learning to overcome weaknesses in images and GIS visualization," *Appl. Sci.*, vol. 11, no. 3, 2021, Art. no. 892.
[20] R. M. Haralick and L. G. Shapiro, *Computer and Robot Vision*, vol. 1. Boston, MA, USA: Addison-Wesley, 1992.
[21] Microsoft, "LightGBM documentation," 2019. [Online]. Available: https://lightgbm.readthedocs.io/en/latest/
[22] J. M. R. S. Appuhamy *et al.*, "Development of an efficient maintenance strategy for corroded steel bridge infrastructures," *J. Bridge Eng.*, vol. 18, no. 6, pp. 464–475, 2013.
[23] K. Karunananda *et al.*, "New combined high and low-cycle fatigue model to estimate life of steel bridges considering interaction of high and low amplitudes loadings," *Adv. Struct. Eng.*, vol. 15, no. 2, pp. 287–302, 2012.
[24] C. N. N. Karina *et al.*, "Tensile strength prediction of corroded steel plates by using machine learning approach," *Steel Composite Struct.*, vol. 24, pp. 635–641, 2017.
[25] P. J. Chun *et al.*, "Development of a machine learning-based damage identification method using multi-point simultaneous acceleration measurement results," *Sensors*, vol. 20, no. 10, 2020, Art. no. 2780.

Pang-jo Chun received the B.E. and M.E. degrees from the Faculty of Engineering, The University of Tokyo, Tokyo, Japan, in 2003 and 2005, respectively, and the Ph.D. degree from Wayne State University, Detroit, MI, USA, in 2010.

He was a Research Associate with Yonsei University from June 2010 to November 2010, and then moved to Ehime University as an Assistant Professor. He worked with Ehime University until March 2018, and since April 2018, he has been a Project Associate Professor with the Graduate School of Engineering, The University of Tokyo. His research interest is in civil engineering, especially in the application of ICT technology to the maintenance and management of bridges and tunnels. He received the Telford Premium Award from the Institute of Civil Engineers in 2020, and several other. He is a member of JSCE and JCI.

Shogo Hayashi is currently working toward the Ph.D. degree with Ehime University, Matsuyama, Japan.

Since, 2008, he has been working with West Nippon Expressway Engineering Shikoku Company Limited, Takamatsu, Japan. His research interest is in civil engineering, especially in the maintenance and management technologies for concrete structures. He received the Intelligence, Informatics and Infrastructure Excellent Paper Award from JSCE in 2020, and several other. He is a member of JSCE and JCI.